



Study of heat transfer for a pair of rectangular jets impinging on an inclined surface

Subrata Roy ^{*}, Paresh Patel ¹

Department of Mechanical Engineering, Kettering University, 1700 West Third Avenue, Flint, MI 48504-4898, USA

Received 5 July 2001; received in revised form 24 July 2002

Abstract

Critical design parameters in jet impingement heat transfer like nozzle hydraulic diameter, jet angle and velocity, physical properties of the fluid, and nozzle-to-target plane spacing are the subject. This paper identifies the dominant fluid-thermal characteristics of a pair of rectangular air jets impinging on an inclined surface. Heat transfer modes and flow characteristics are studied with eight different Reynolds numbers ranging from 500 to 20 000. Local and average Nusselt numbers are evaluated with two different boundary conditions on three specified lines located on the inclined surface. The correlation between stagnation Nusselt number and Reynolds number is presented. Turbulent intensity and wall y^+ distributions are compared on three lines parallel to the incline. The effect of jet impingement angle on local and average Nusselt number is also documented. Finally, a correlation between the average Nusselt number, nozzle exit Reynolds number and the jet angle is documented.

© 2002 Elsevier Science Ltd. All rights reserved.

Keywords: Climate control; CFD; Inclined surface; Impinging jets; Rectangular slots

1. Introduction

Jet impingement heat transfer has been employed in many practical applications for cooling and drying because of its easy implementation and high heat transfer rate. Examples include turbine blade film cooling, bearing cooling, electronics cooling, vehicle windshield deicing/defogging, drying of paper, and glass tempering. In many of these applications, the Nusselt number (Nu) distribution resulting from the jet attachment to the target plane, the trajectory and physical properties of the jet are critical design parameters. The specific interest is air issuing from two rectangular openings and impinging upon an inclined surface that is common in vehicle windshield climate control application.

Impingement of single and multiple jets on surface has been extensively investigated in the literature [1–16,21,22]. Impingement of single circular jet on perpendicular and inclined plate in Lamont and Hunt [1] showed surface pressure distribution on entire impingement region for varying pressure ratios and plate angles ranging from 30° to 90°. Bernard et al. in [2] used various experimental techniques to describe the flow of several jets impinging on a plane wall. Polat et al. [3] presented a review of numerical studies related to axisymmetric impinging jets. More reviews were documented by Martin [4], and Downs and James [5]. Lee et al. [6] showed local heat transfer from an elliptical jet impingement on a flat plate. An array of elliptical jets has been studied extensively by Arjocu and Liburdy [7] to understand the dominant local heat transfer modes for low Reynolds number (Re) such as 300 and 1500, while Martin [8] has identified optimum impingement and separation distances for heat transfer for a wider flow range, $2500 \leq Re \leq 4000000$. The effects of Re , nozzle geometry and the separation distance were also studied by Colucci and Viskanta [9].

^{*} Corresponding author. Tel.: +1-810-762-9949; fax: +1-810-762-7860.

E-mail addresses: sroy@kettering.edu (S. Roy), patel@erc.msstate.edu (P. Patel).

¹ Currently at Mississippi State University.

Nomenclature

C_i	coefficients
E	specific enthalpy
k	turbulent kinetic energy
L_e	characteristic length
p	static pressure
Pr	Prandtl Number
S_{ij}	mean strain tensor
t	time
T	temperature
T_u	turbulence level
u_i	Cartesian velocity component
u_τ	wall shear velocity
x_i	spatial coordinates
y^+	inner variable

Greek symbols

ε	dissipation rate of turbulent kinetic energy
---------------	--

μ_t	eddy viscosity
μ	viscosity
ρ	density
τ_{ij}	stress tensor
δ_{ij}	Kronecker delta

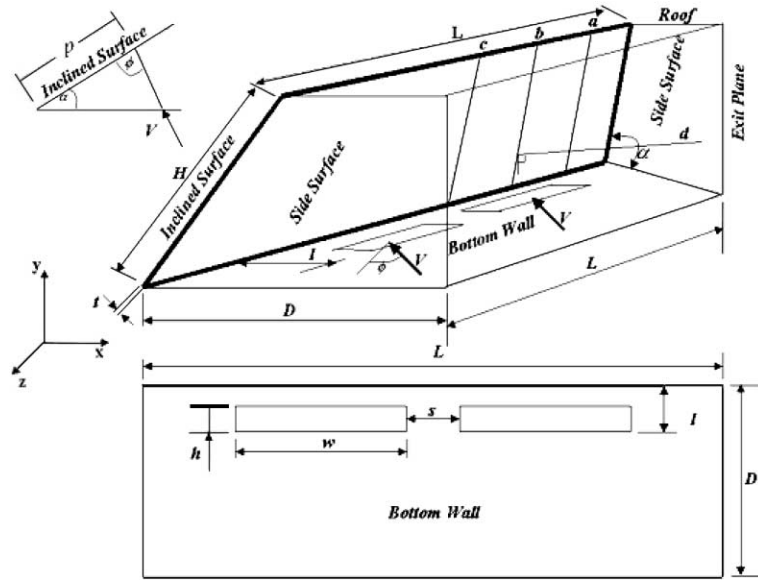
Subscripts

avg	average
eff	effective
in	inlet (at nozzle exit)
i, j	direction of special derivatives
k	mean velocity
stg	stagnation condition
τ	shear stress based variable
w	wall

Pan and Webb [10] studied local heat transfer details of the circular jet array impingement. Metzger et al. [11] has investigated the effect of Prandtl number (Pr) on jet impingement heat transfer characteristics while Rahman et al. [12] has identified conjugate heat transfer during free jet impingement of a high Pr fluid. Leland and Pais [13] obtained heat transfer coefficients for high Pr fluid ranging from 48 to 445 and jet Re of 109 to 8592. Morris et al. [14] has studied local heat transfer coefficient distribution on the plate due to a normally impinging jet of Reynolds Number ranges from 8500 to 13 000. Recently, Roy et al. [15,16] has compared numerical and experimental results for temperature and local heat transfer coefficient distribution on the two rectangular jets impinging upon an inclined surface.

In this paper, we study the jet impingement flow characteristics and investigate the effect of Reynolds number and jet angle on local and average Nu , turbulence intensity (TI) and wall y^+ . Fig. 1 describes schematic of the jet, the inclined plane and its association with the control volume bounded by five other surfaces. All necessary dimensions are given in the figure. Air jets are issued at temperature T_j , with streamwise and crosswise angles (ϕ and β) from the nozzle exit plane, through two rectangular openings ($h \times w$) impinging upon the target plane of thickness t with known material properties. These openings are centered on the length L of the bottom wall. The target plane is inclined at an angle of α . The mean velocity of the jet V depends on the jet Reynolds number and the hydraulic diameter of the inlet nozzle. For this geometry, the impingement point, i.e., the intersection of the jet axis and the inclined surface is at a distance p away from the crotch, $p = (l - (h/2))(\cos \alpha + (\sin \alpha / \tan \phi))$.

Three lines a, b and c with constant z -coordinate 0.3733, 0.5233 and 0.7233 m, respectively, are selected along the height H of the inclined plane for understanding heat transfer process and flow characteristics. These lines coincide with the plane between the jet and side surface, axis of the jet, and between the jets. The horizontal line d with constant y -coordinate of 0.072 m, starts from the point where the jet axis impinges on the surface for $\phi = 60^\circ$ and ends on a point of the exit plane as shown in Fig. 1. Heat transfer process in the computational domain is investigated by using a finite volume based commercial code FLUENT® [17]. The three-dimensional computational model is analyzed with renormalized group (RNG) $k - \varepsilon$ turbulence closure model of Yakhot and Orszag [18] to understand fluid-thermal characteristics in jet impingement heat transfer. Comparison between the local and average Nu on the surface, and TI and wall y^+ distribution at a distance parallel to the surface are reported for two different boundary conditions. The correlation between stagnation Nu and Re is presented. Nusselt number, TI and wall y^+ distribution over the inclined surface are compared for eight different Reynolds numbers ($Re = 500, 1500, 5000, 7500, 10\,000, 12\,500, 15\,000$ and $20\,000$) for air ($Pr = 0.7$). The effect of jet angle on the impingement heat transfer is also discussed for Reynolds numbers 5000, 10 000 and 20 000. The angle ϕ is varied from 30° to 90° in steps of 15° in the xy -plane and then for $\phi = 75^\circ$, the sweep angle β is varied from 5° to 15° (outward direction) and -5° to -15° (inward direction) in the yz -plane. The jet openings are in plane with the bottom wall for all these experiments. The effect of jet impingement angle on local and average Nu , TI and wall y^+ is then reported. Finally, a correlation between the



Length of inclined surface, L	1.447 m
Width of inclined surface, H	0.791 m
Surface inclination angle, α	30°
Inclined surface thickness, t	0.006 m
Location of the nozzle, l	0.134m
Length of nozzle exit plane, h	0.019 m
Width of nozzle exit plane, w	0.241 m
Jet angle, ϕ (on x - y plane)	30° to 90°
Sweep angle, β (on y - z plane)	0° to $\pm 15^\circ$
Width of bottom wall, D	0.896 m
Distance between nozzle exit planes, s	0.127 m

Fig. 1. Schematic of the computational domain.

average Nusselt number, exit Reynolds number and the jet impingement angle ϕ is presented.

2. Theoretical formulation

2.1. Governing equations

The three-dimensional incompressible Navier–Stokes form for a steady state assumption may be written as,

Mass (continuity) equation:

$$\frac{\partial u_i}{\partial x_i} = 0 \tag{1}$$

Momentum equation:

$$\rho u_j \frac{\partial u_i}{\partial x_j} + \frac{\partial p}{\partial x_i} - \frac{\partial \tau_{ij}}{\partial x_j} = 0 \tag{2}$$

Energy equation:

$$\frac{\partial}{\partial x_j} (\rho u_j E - u_i \tau_{ij}) = 0 \tag{3}$$

where the stress tensor τ_{ij} ,

$$\tau_{ij} = \left[\mu \left(\frac{\partial u_i}{\partial x_j} + \frac{\partial u_j}{\partial x_i} \right) \right] - \frac{2}{3} \mu \frac{\partial u_i}{\partial x_i} \delta_{ij}$$

2.2. Turbulence modeling

There are several models for turbulent flow simulation to numerically close the product of fluctuating components of state variables or subgrid terms in (1)–(3). One such RNG based standard $k - \epsilon$ turbulence model of Yakhot and Orszag [18] contains the following

two equations, one for turbulence kinetic energy k and the other for its dissipation rate ε , respectively,

$$\frac{\partial}{\partial x_i} \left[\left(\mu + \frac{\mu_t}{Pr_k} \right) \frac{\partial k}{\partial x_i} \right] + \left(2\mu_t S_{ij} - \frac{2}{3} \rho k \delta_{ij} \right) \frac{\partial u_j}{\partial x_i} = \rho \varepsilon \quad (4)$$

and

$$\begin{aligned} \frac{\partial}{\partial x_i} \left[\left(\mu + \frac{\mu_t}{Pr_k} \right) \frac{\partial \varepsilon}{\partial x_i} \right] + C_{1\varepsilon} \frac{\varepsilon}{k} \left(2\mu_t S_{ij} - \frac{2}{3} \rho k \delta_{ij} \right) \frac{\partial u_j}{\partial x_i} \\ = C_{2\varepsilon} \rho \frac{\varepsilon^2}{k} \end{aligned} \quad (5)$$

In the above equations, the left hand side shows the diffusion and generation terms and the right hand side involves dissipation rate terms. The turbulent viscosity is modeled as $\mu_t = C_\mu \rho k^2 / \varepsilon$, where $C_\mu = 0.0845$ (Lam [19]). The standard coefficients are $C_{1\varepsilon} = 1.42$ and $C_{2\varepsilon} = 1.68$. Accurate computation of the turbulent flow strongly depends on the local grid generation especially in the near wall region where the shear layer forms. In this region, the mesh measure can be computed as,

$$y^+ = \frac{\rho u_\tau f(y)}{\mu} \quad (6)$$

where the wall shear velocity $u_\tau = \sqrt{\tau_w / \rho}$ and $f(y)$ is the normal distance from the wall.

The turbulent viscosity is not a fluid property, but rather a property of the flow field. Its value is added to the molecular viscosity and yields an effective viscosity, μ_{eff} , which is used in the computational model. The k and ε at the inlet are calculated from the following expressions:

$$k_{\text{in}} = \frac{3}{2} (T_u \cdot u)^2 \quad \varepsilon_{\text{in}} = \frac{k_{\text{in}}^{3/2}}{L_e} \quad (7)$$

where T_u is the turbulence level and L_e is a characteristic length based on the nozzle exit.

Eqs. (1)–(5) constitute a system of non-linear algebraic equations. The system is linearized by relaxation. A second-order accurate streamline upwinding technique is employed for stabilizing numerical iterations. The pressure corrections are used to correct the pressure and the velocities. This predictor-corrector procedure constitutes an iteration. The solution is declared convergent when the maximum residual for each of the state variable becomes smaller than a convergence criterion of ϵ . Here, the convergence of a solution vector \mathbf{U} on node n is defined as the norm:

$$\frac{\|\mathbf{U}_n - \mathbf{U}_{n-1}\|}{\|\mathbf{U}_n\|} \leq \epsilon$$

We selected $\epsilon = 10^{-3}$ for continuity, momentum, turbulence kinetic energy and its dissipation rate equations and $\epsilon = 10^{-6}$ for the energy equation.

2.3. Boundary conditions

Two different boundary condition cases (A and B) are utilized to analyze the fluid thermal system. In the first case, the roof, side walls, bottom wall and back wall of the control volume are considered as typical wall boundary conditions. Here onwards, this will be called ‘Case A’. In the other, all boundaries except for the inclined plane, bottom wall and inlet jets are pressure outlet i.e. atmospheric pressure boundary condition. Here onwards, we call this ‘Case B’. Details of the imposed boundary condition for cases A and B are given in Table 1 (Panels A and B), respectively. The inclined plane is always considered as no-slip wall where a convective boundary condition with constant temperature of 273 K and a heat transfer coefficient of 35 W/m² K is applied on the outer surface. Air jets are issued at 293 K from the nozzle exit plane with a plug flow velocity \vec{V} that was imposed based on $500 \leq Re \leq 20000$. According

Table 1
Prescribed boundary conditions for Case A (Panel A) and Case B (Panel B)

Boundary	U	v	w	T	p	k	ε
<i>Panel A</i>							
Inclined plate	0	0	0	273K, 35 W/m ² K	$\partial p / \partial n = 0$	$\partial k / \partial n = 0$	ε_w
Nozzle	Prescribed uniform profile			293K	$\partial p / \partial y = 0$	k_{in}	ε_{in}
Bottom	0	0	0	$\partial T / \partial y = 0$	$\partial p / \partial y = 0$	$\partial k / \partial y = 0$	ε_w
Sides	0	0	0	$\partial T / \partial z = 0$	$\partial p / \partial z = 0$	$\partial k / \partial z = 0$	ε_w
Roof	0	0	0	$\partial T / \partial y = 0$	$\partial p / \partial y = 0$	$\partial k / \partial y = 0$	ε_w
Exit	$\partial u / \partial x = 0$	$\partial v / \partial x = 0$	$\partial w / \partial x = 0$	$\partial T / \partial x = 0$	$\partial p / \partial x = 0$	$\partial k / \partial x = 0$	$\partial \varepsilon / \partial x = 0$
<i>Panel B</i>							
Inclined plate	0	0	0	273K, 35 W/m ² K	$\partial p / \partial n = 0$	$\partial k / \partial n = 0$	ε_w
Nozzle	Prescribed uniform profile			293K	$\partial p / \partial y = 0$	k_{in}	ε_{in}
Bottom	0	0	0	$\partial T / \partial y = 0$	$\partial p / \partial y = 0$	$\partial k / \partial y = 0$	ε_w
Sides	$\partial u / \partial z = 0$	$\partial v / \partial z = 0$	$\partial w / \partial z = 0$	$\partial T / \partial z = 0$	$\partial p / \partial z = 0$	$\partial k / \partial z = 0$	$\partial \varepsilon / \partial z = 0$
Roof	$\partial u / \partial y = 0$	$\partial v / \partial y = 0$	$\partial w / \partial y = 0$	$\partial T / \partial y = 0$	$\partial p / \partial y = 0$	$\partial k / \partial y = 0$	$\partial \varepsilon / \partial y = 0$
Exit	$\partial u / \partial x = 0$	$\partial v / \partial x = 0$	$\partial w / \partial x = 0$	$\partial T / \partial x = 0$	$\partial p / \partial x = 0$	$\partial k / \partial x = 0$	$\partial \varepsilon / \partial x = 0$

to the jet impingement angle (ϕ and β) the u , v and w components of plug flow velocity \vec{V} are calculated and applied at the inlets. Corresponding k and ϵ values at the inlet are calculated via (7). The nozzle exit is in plane with the bottom wall for all variations of ϕ and β .

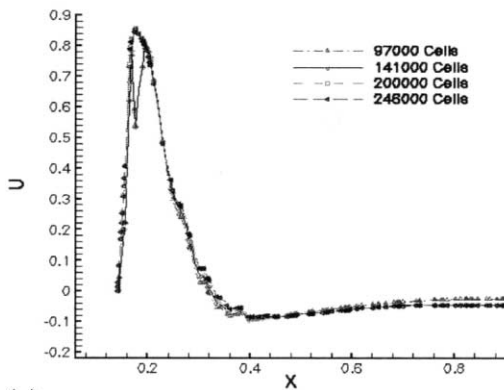
3. Results and discussion

Fig. 1 shows schematic of the computational domain which has been discretized in to tetrahedral finite volumes using commercial modeling code Hypermesh[®] 4.0 [20]. The three-dimensional Navier-Stokes equations (1)–(5) are then solved using Fluent[®] 5.2 [17] for flow, energy and turbulence closure. The Nusselt number distribution on three lines a, b, c in Fig. 1, and TI and y^+ distribution at a normal distance of 0.003 m parallel to these lines are investigated in this section. Corresponding material properties of the inclined glass surface and its associated control volume of air are shown in Table 2.

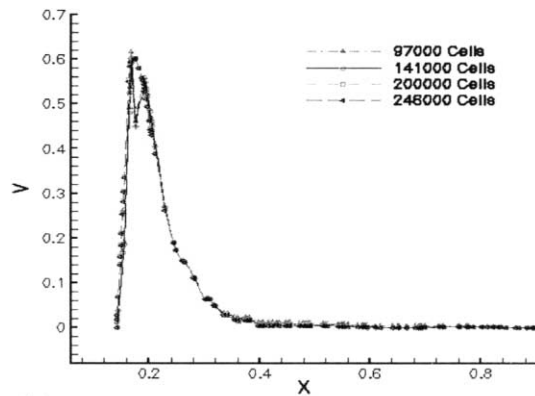
Table 2
Material properties used in the numerical simulation

	Air	Glass
Density (kg/m ³)	1.225	2500
Specific heat (J/kg K)	1006.43	750
Thermal conductivity (W/m K)	0.0242	1.4
Viscosity (kg/m s)	1.7894e–5	

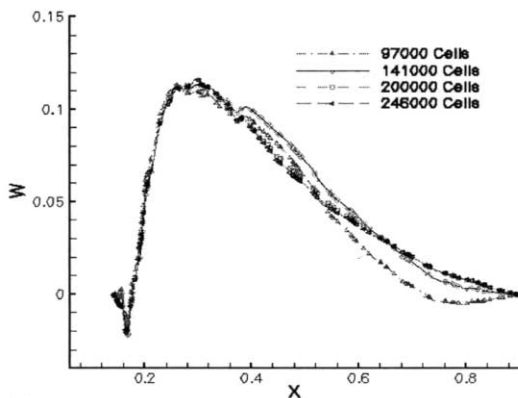
A mesh independence study of velocity components plotted for this line d with four different mesh sizes of 97 000 cells, 141 000 cells, 200 000 cells and 246 000 cells, Fig. 2a–d, established the moderate 200 000 tetrahedral cells as the optimum mesh. The inlet conditions for this mesh study were uniform velocity profiles based on $Re = 12500$ for both openings. Fig. 2d plots the zoomed-in comparison of v -velocity near shear layer region demonstrating that nearly grid independent results can be obtained on the moderate 200 000 cells grid. It should be noted here, that grid independent solution with respect to turbulence variables has not been achieved, but the difference on the results from the moderate and fine



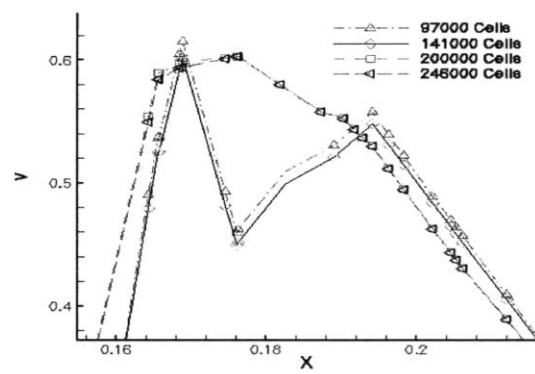
(a) u velocity comparison on different mesh



(b) v velocity comparison on different mesh



(c) w velocity comparison on different mesh



(d) Zoomed in v velocity near the peak

Fig. 2. Mesh independence study on line d for $Re = 12500$ with $\phi = 60^\circ$ and $\beta = 0^\circ$.

mesh is small (less than 3% of moderate solution peak) and use of any finer mesh would only increase the computational cost. Hence hereafter, our computational mesh consists of 200 000 cells.

Fig. 3a describes how the fluid comes out of the nozzle and impinges upon the surface and divides into

major and minor flows for boundary condition A. Significant portion of the incoming fluid attaches the wall and moves upward eventually going towards downstream and creating a recirculation associated with complex multiple vortex structure in the computational domain while rest of the incoming fluid creates a smaller

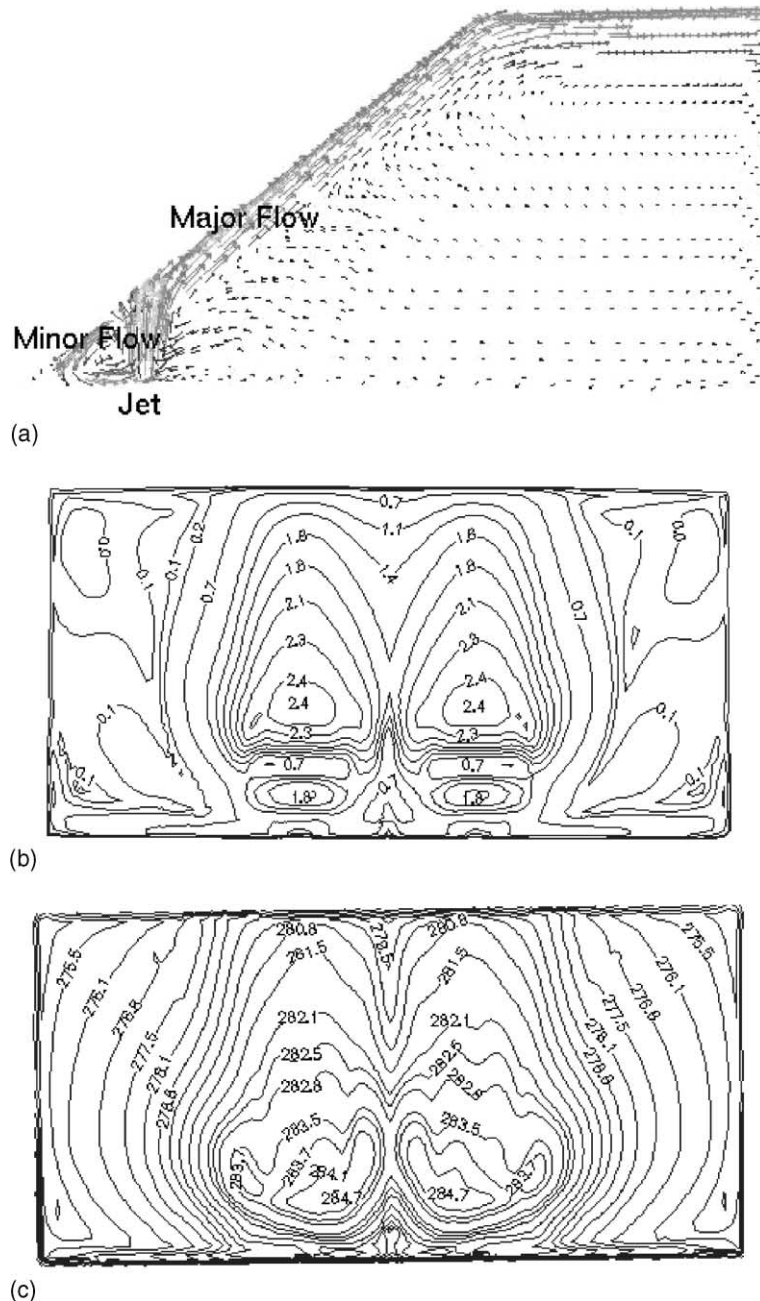


Fig. 3. Simulation results for $Re = 20000$ with Case A at $\phi = 60^\circ$ and $\beta = 0^\circ$. (a) Velocity vectors plotted on the xy -plane at $z = 0.5233$ m; (b) speed (m/s) contour on a parallel plane at normal distance of 0.01 m next to inclined wall; (c) static temperature (K) on the inside of the inclined surface.

wake upstream, towards the crotch (bottom left in Fig. 3a). For $Re = 20000$, Fig. 3b shows the speed contours close to the inclined surface at a distance of 0.01 m demonstrating the stagnation region and shear layers that affects the fluid flow structure. A pair of turbulent, incompressible, rectangular jets is impinging on the inclined wall. Each jet creates a stagnation zone about the impingement location, and then spreads in all the direction attaching the wall. The major and minor flows that follow generate shear layers. Temperature distribution on inclined wall is shown in Fig. 3c that plots symmetric contour patterns for $Re = 20000$ with the highest temperature in the stagnation region where the jet impinges upon the wall. Near this region the heat diffusion is dominant. The temperature decreases in the rest of the wall through convective heat transfer in the shear layer.

After impingement, each jet creates a pair of counter rotating vortices in the crosswise direction. It is obvious that the jet spreads more due to these bound vortices, covering a larger cross-section. This is the result of the bound vortices being confined in a smaller space, in-

ducing larger crosswise components of velocity and thus aiding the spread of the jet. The flow coming out of the hole in the form of a jet is subjected to bending due to the impingement and in the process reducing significantly the effect of the boundary layer thickness. The vorticity associated with the wake side of the jet produces a pair of bound vortices. Fig. 4 documents these bound vortices created between the jets on the vertical plane cutting through the inlet jet for $Re = 20000$ at $x = 0.144$ m with $\phi = 60^\circ$ and $\beta = 0^\circ$.

Fig. 5 shows particle track from inlet colored by velocity magnitude, based on $Re = 20000$, in the computational domain (color figures for this paper are available at <http://meweb.kettering.edu/publications/sroy/ijhmt2.pdf>). For Case A, Fig. 5a shows formation of small bound vortices in between two rectangular inlet openings because of large velocity magnitude, while after impingement of the jet with solid surface it creates a smaller upstream wake and a larger wake in the downstream region. The three dimensionality of the flow field is evident. Fig. 5b also shows the same for Case B, but does not display any three-dimensional flow recirculation



Fig. 4. Velocity vector distribution on the central cutting plane shows strong bound vortices between the jets for $Re = 20000$ with $\phi = 60^\circ$ and $\beta = 0^\circ$.

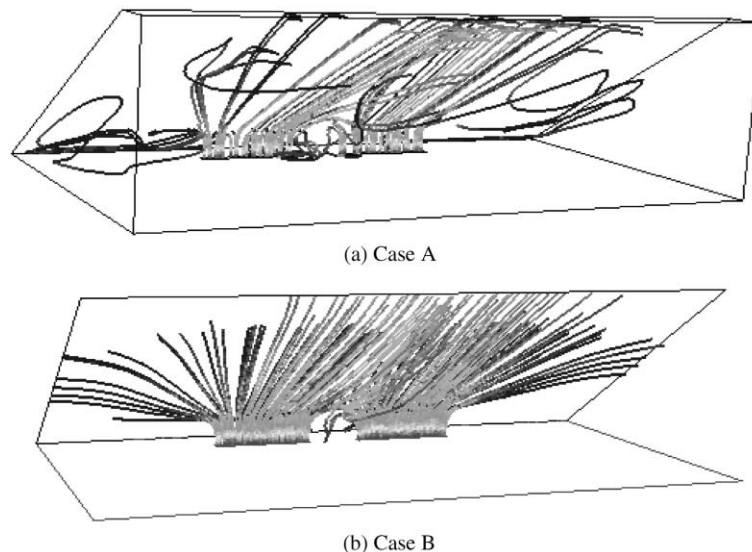


Fig. 5. Path lines showing the particle tracks in the computational domain with two different boundary conditions for $Re = 20000$ with $\phi = 60^\circ$ and $\beta = 0^\circ$.

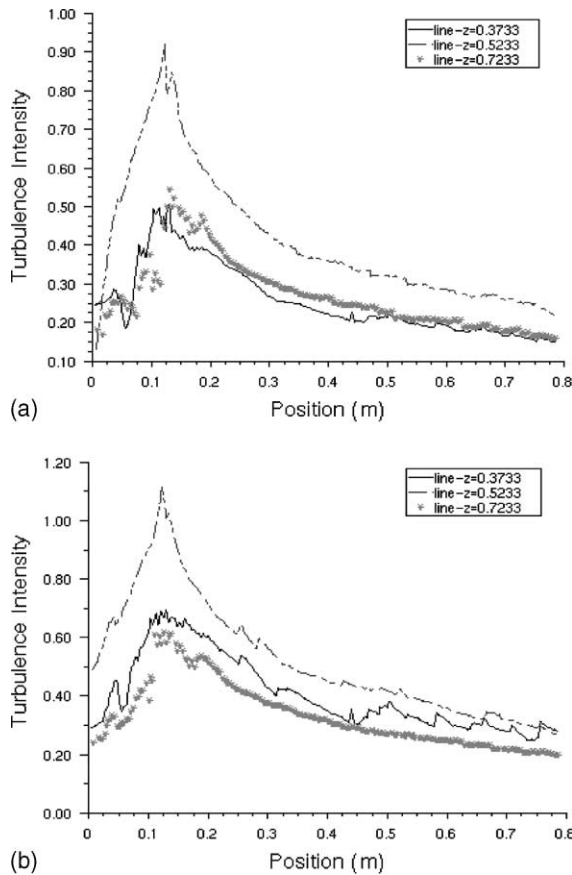


Fig. 6. Comparison of TI distribution parallel to lines a, b, c at a normal distance 0.003 m near the inclined surface for two boundary conditions for $Re = 20000$ with $\phi = 60^\circ$ and $\beta = 0^\circ$: (a) Case A; (b) Case B.

except for bound vortices formation on the $y-z$ plane between the jets.

Inlet TI plays a critical role in identifying the level of turbulence kinetic energy in the solution domain. Fig. 6 shows TI distribution on lines parallel to a (line $z = 0.3733$ m), b (line $z = 0.5233$ m) and c (line $z = 0.7233$ m) at a normal distance of 0.003 m for $Re = 20000$. The distribution remains high about the stagnation region showing mean velocity gradient is the highest at that point and sharply decreases in the nearby region where the shear layer forms. TI is generally 20% higher for Case B than for Case A. The non-dimensional y^+ is a function of wall shear stress. Fig. 7 shows the distribution of wall y^+ on the lines parallel to a (line $z = 0.3733$ m), b (line $z = 0.5233$ m) and c (line $z = 0.7233$ m) at a normal distance of 0.003 m to demonstrate wall shear stress distribution. The y^+ is spatially fluctuating but its peak is about the stagnation point and decreases slowly in its nearby region. This means maximum wall shear stress is being produced at the stagnation point and then

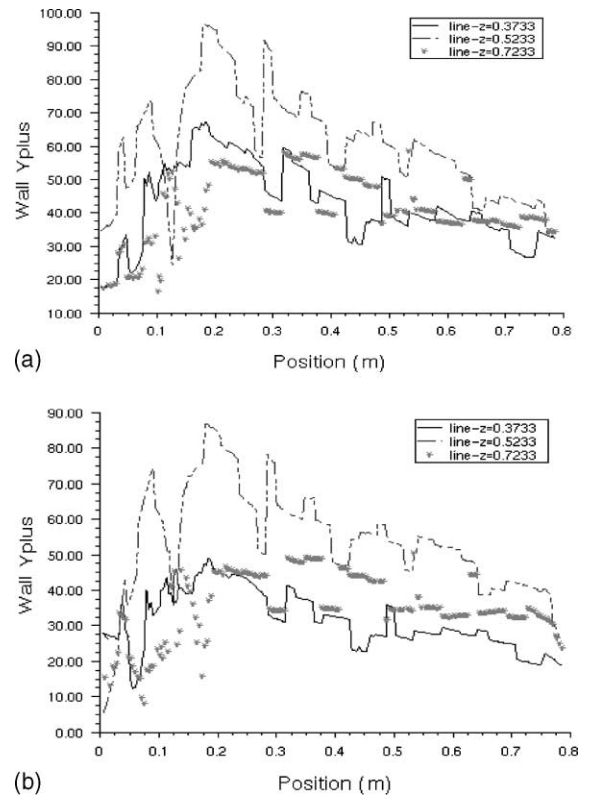


Fig. 7. Comparison of y^+ distribution parallel to lines a, b, c at a normal distance 0.003 m near the inclined surface for two boundary conditions for $Re = 20000$ with $\phi = 60^\circ$ and $\beta = 0^\circ$: (a) Case A; (b) Case B.

it decays slowly in the nearby region. Moreover, it is nearly 10% lower for Case B than for Case A, which demonstrates generation of higher wall shear stress for Case A than in Case B for the same Reynolds Number.

Fig. 8 shows the comparison of local Nu distribution on lines a (line $z = 0.3733$ m), b (line $z = 0.5233$ m) and c (line $z = 0.7233$ m) for $Re = 20000$, with boundary condition cases A and B for the control volume. Nu distribution gives better idea of jet impingement heat transfer through the surface. In general, the local Nu for Case A is about 30% higher than that in Case B. The Nu peaks at the stagnation point and then decreases in its nearby region where shear layer forms. A careful observation of Fig. 8 reveals that the stagnation point is at a position about 0.12 m away from the crotch, displaced from the intersection of the jet axis ($p = 0.1437$ m for $\alpha = 30^\circ$ and $\phi = 60^\circ$) towards the crotch. This is consistent with the reported literature [21]. The discrepancy is due to the fact that the jets coming out of the opening are subjected to bound vortices and in the process significantly bend downward.

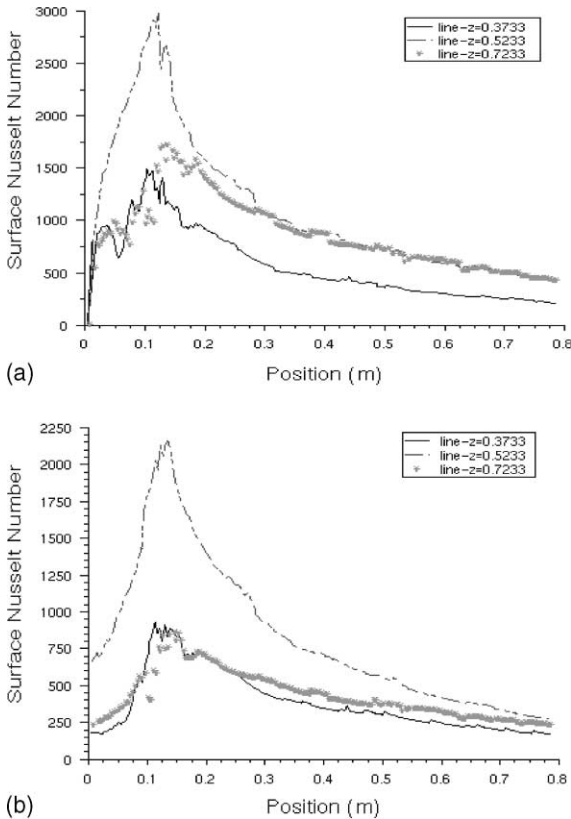


Fig. 8. Comparison of Nusselt number distribution on the surface along lines a, b, c for two boundary conditions for $Re = 20000$ with $\phi = 60^\circ$ and $\beta = 0^\circ$: (a) Case A; (b) Case B.

Fig. 9 shows the trend of average Nusselt number (Nu_{avg}) on the surface for different Re with boundary condition cases A and B. The average Nu is computed on the inside of the inclined surface of area Γ as:

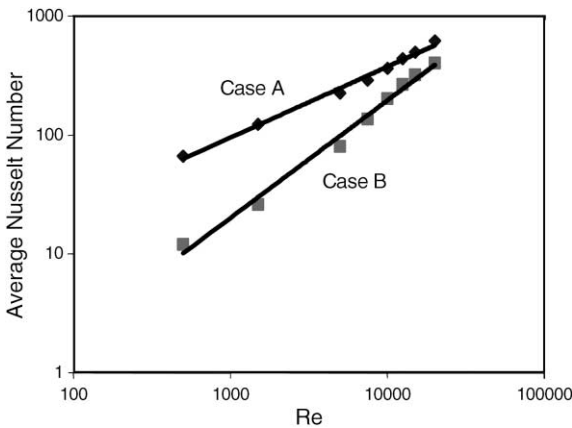


Fig. 9. Effect of boundary condition and flow characteristics on heat transfer process with $\phi = 60^\circ$ and $\beta = 0^\circ$.

$$Nu_{avg} = 1/\Gamma \int_{\Gamma} Nu d\Gamma \tag{8}$$

In general, Nu_{avg} increases as the Re increases. It is also higher for Case A than for Case B. The jet-vortex interaction appears to have a significant effect on heat transfer. For all Re , the peak Nusselt number in Case A is always higher than that for Case B. This is primarily due to the fact that less energy is lost in Case A than in B. Also peak Nu increases as Re increases. The trendline shows for Case A,

$$Nu_{avg} = 1.54Re^{0.5962} \approx 1.54Re^{0.6} \tag{9a}$$

while for Case B, the relationship is

$$Nu_{avg} = 0.021Re^{0.9888} \approx 0.02Re \tag{9b}$$

Another important aspect is the stagnation Nusselt number and its functional relation to the flow parameters. Similar studies have been done by Lonney and Walse [22] for an isothermal two-dimensional turbulent jet impinging on a heated flat plate placed at right angle for different values of Re and height to width ratio of nozzle outlet plane (h/b). They proposed correlation to predict stagnation Nusselt number (Nu_{stg}) based on two-dimensional analysis,

$$Nu_{stg} = 1.2Re^{0.58}(h/b)^{-0.62} \pm 5\%$$

where $14 < h/b < 60$ and $2000 < Re < 50000$. In comparison, Fig. 10 documents stagnation Nu for different Re for a pair of laminar and turbulent slot jets impinging at an angle $\phi = 60^\circ$ and $\beta = 0^\circ$ using a three-dimensional model. Based on air ($Pr = 0.7$), the trendline shows our proposed relationship between Nu_{stg} and Re as

$$Nu_{stg} = 11.5Re^{0.63} \tag{10}$$

The obvious difference is due to the fact that in [22] the two-dimensional domain has all sides open boundary condition, and the correlation (10) is found based on three-dimensional analysis with Case A boundary condition.

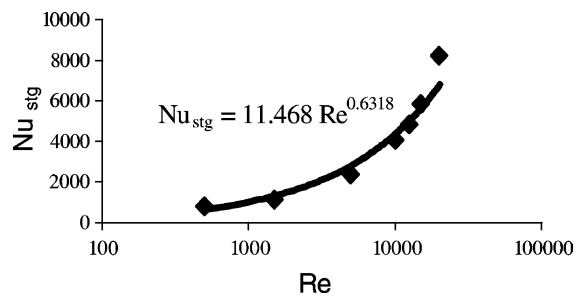


Fig. 10. Comparison of Nu_{stg} vs Re for Case A and jet angles $\phi = 60^\circ$, $\beta = 0^\circ$.

Fig. 11a–c show local Nusselt number, TI and wall y^+ distribution on line b for different Reynolds numbers

for Case A. Heat transfer is maximum through the shear layer region as discussed earlier and peak of Nu , TI and

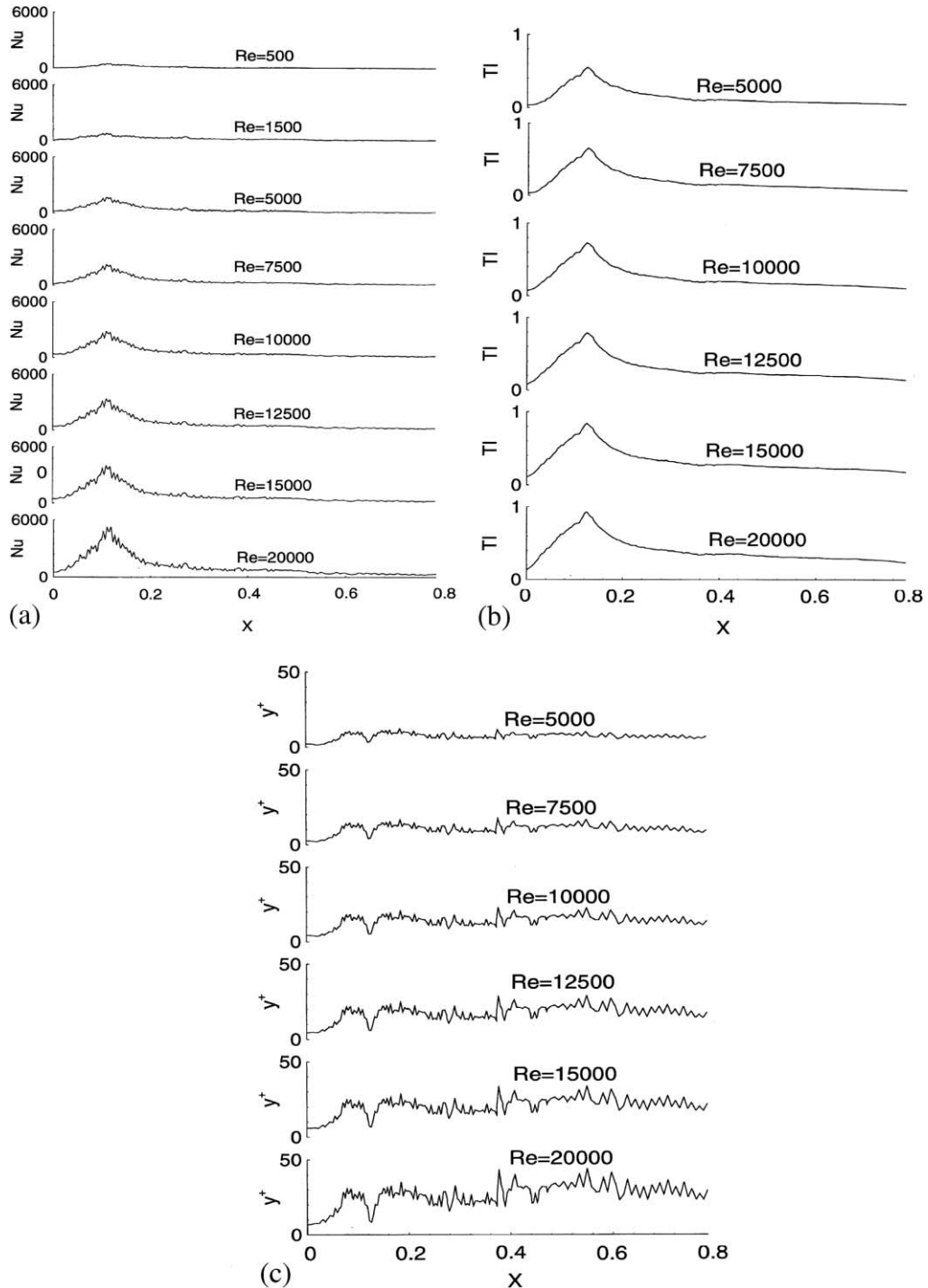


Fig. 11. Effect of Reynolds number on (a) local Nusselt number along b on the inside of the inclined surface; and (b) TI and (c) y^+ distributions at a normal distance of 0.003 m parallel to the incline with $\phi = 60^\circ$ and $\beta = 0^\circ$.

y^+ increases as Re increases. The local Nu plot in Fig. 11a for $5000 \leq Re \leq 20000$, demonstrates that at the stagnation point the diffusive heat transfer is dominant

and in its nearby region the convective heat transfer is dominant because of higher velocity gradient. The TI plot in Fig. 11b for $5000 \leq Re \leq 20000$ shows similar

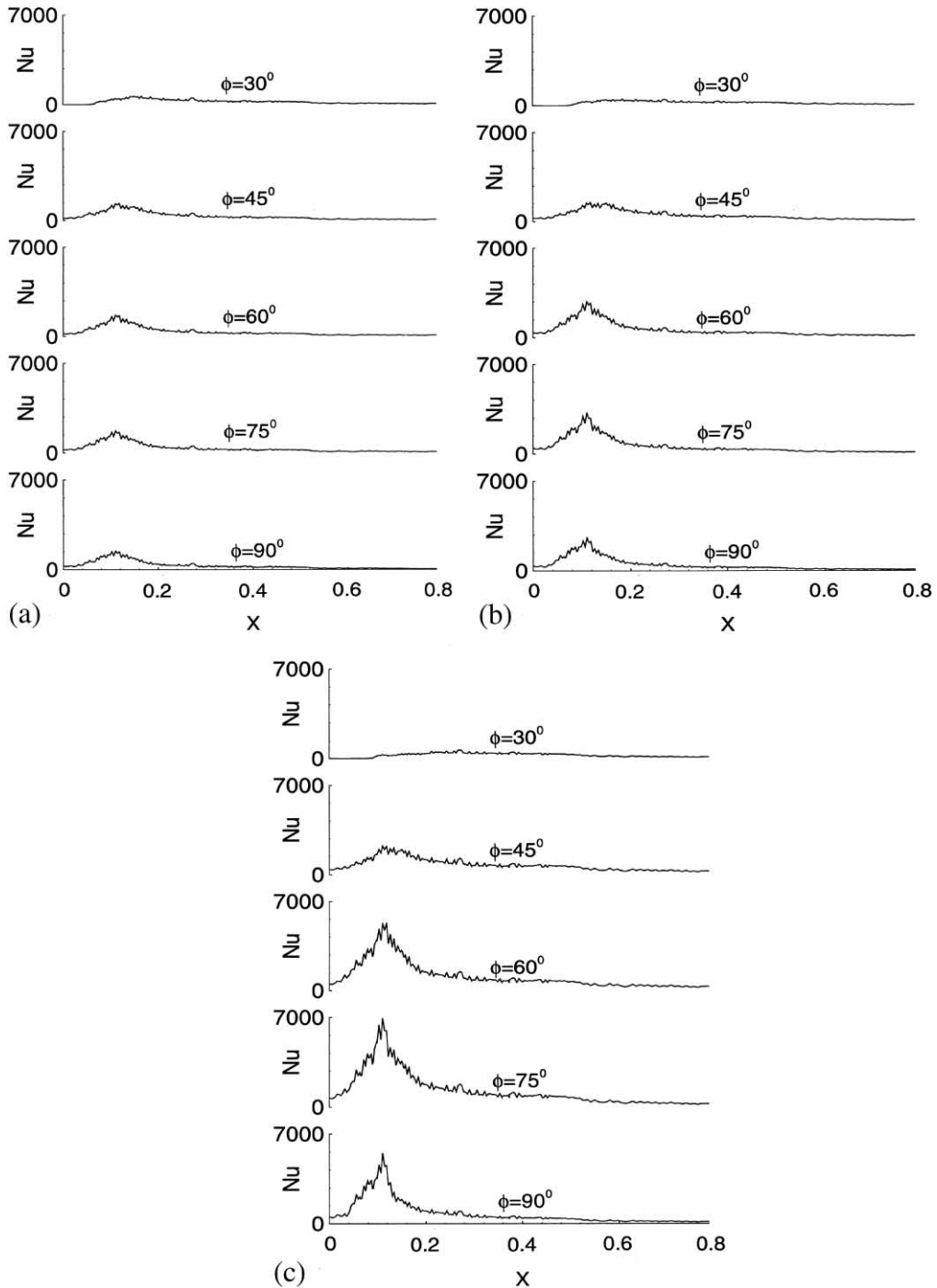


Fig. 12. Effect of jet angle ϕ on local Nu distribution along line b on the inside of the inclined surface: (a) $Re = 5000$, (b) $Re = 10000$ and (c) $Re = 20000$ with $\beta = 0^\circ$.

trend. However, the wall y^+ distribution on line b represents high wall shear beyond the stagnation point, Fig. 11c. At a normal distance of 0.003 m from the inclined wall, the spatial fluctuation in y^+ distribution for $5000 \leq Re \leq 20000$ becomes dominant as Re increases possibly demonstrating the presence of

the turbulent flow structure along the jet attachment region.

The angle ϕ is inclination of the jet axis with respect to the inclined surface in the xy -plane as shown in Fig. 1. The effect of ϕ on heat transferring through the inclined wall is reported in Fig. 12a–c by studying the local Nu

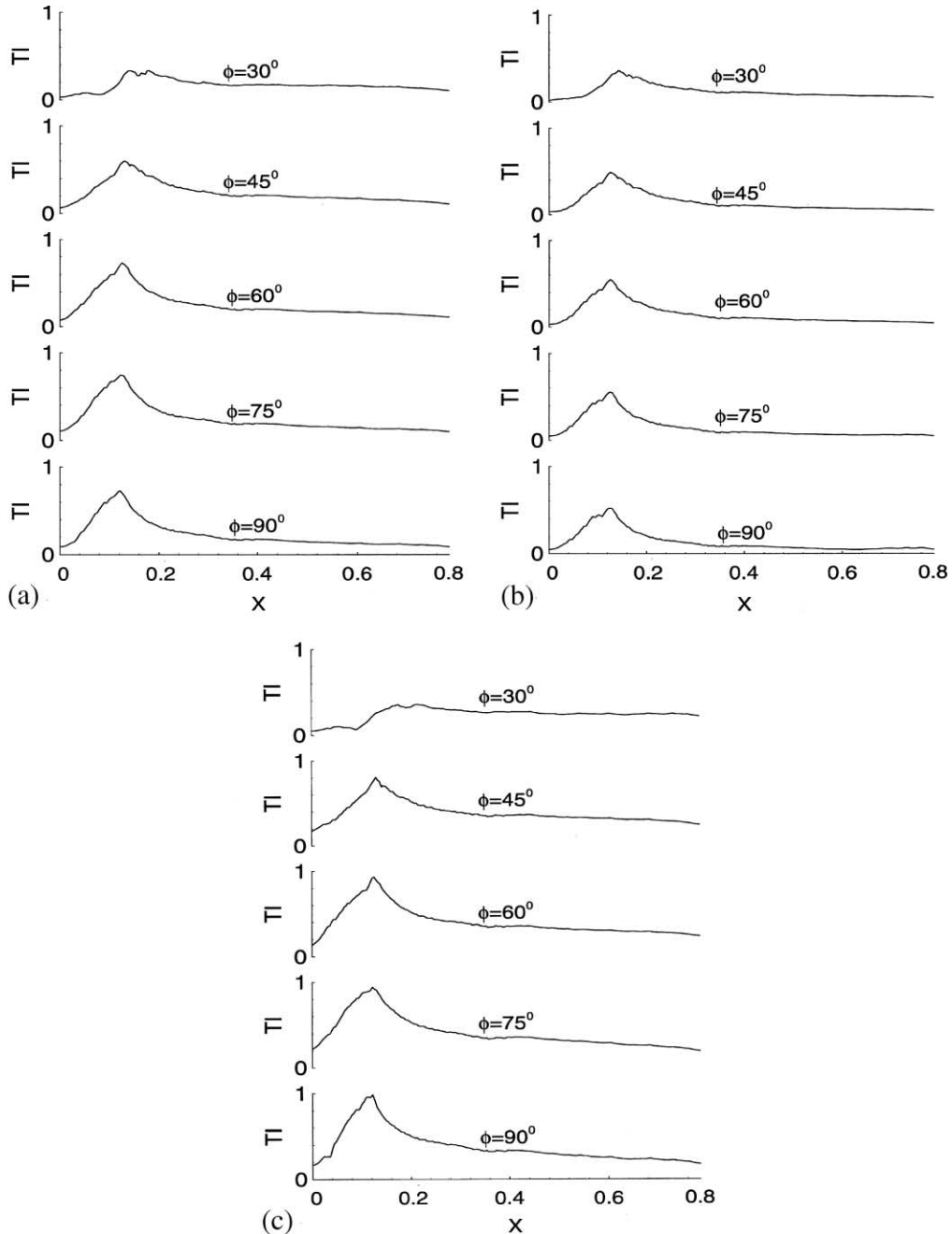


Fig. 13. Effect of jet angle ϕ on turbulent intensity distribution at a normal distance of 0.003 m parallel to line b on the inclined surface: (a) $Re = 5000$, (b) $Re = 10000$ and (c) $Re = 20000$ with $\beta = 0^\circ$.

distribution on line b for $Re = 5000, 10\,000$ and $20\,000$, respectively. Clearly, the effect of jet angle is significant

on heat transfer process for any particular Reynolds number and it is more so for high Re flows as compare

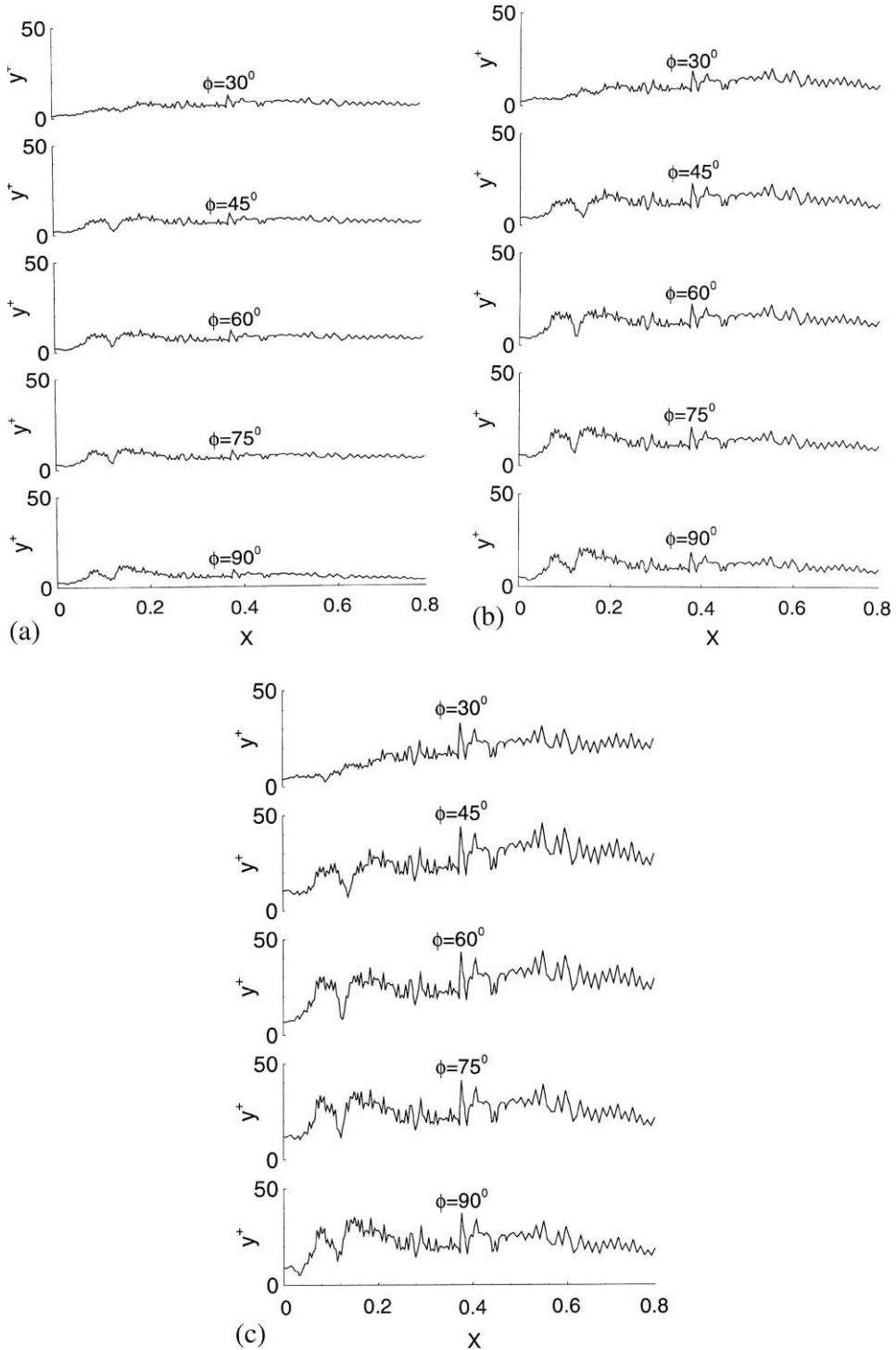


Fig. 14. Effect of jet angle ϕ on y^+ distribution at a normal distance of 0.003 m parallel to line b on the incline: (a) $Re = 5000$, (b) $Re = 10000$ and (c) $Re = 20000$ with $\beta = 0^\circ$.

to low. Moreover, the peak of Nu is shifting towards left because the stagnation point (intersection of the jet axis and solid wall) is moving downwards as jet angle increases from 30° to 90° . The heat transfer is the maximum through this stagnation point. It also shows that the highest value of Nu is attained for $\phi = 75^\circ$ for all Reynolds numbers, specifically for high $Re = 20000$, Fig. 12c.

Similarly, Fig. 13a–c show effect of jet angle (ϕ) on TI distribution along line b for Reynolds number 5000, 10000 and 20000, respectively. The level of turbulent kinetic energy is maximum in the shear layer region and highest at stagnation point which moves towards left as jet angle increase from 30° to 90° . Fig. 13a–c plot the wall y^+ distribution as a function of ϕ for $Re = 5000$, 10000 and 20000, respectively. For $Re = 5000$ in Fig. 14a, the benign y^+ distribution shows less presence of turbulence. As the Re increases from 10000 (Fig. 14b) to 20000 (Fig. 14c), the wall shear becomes dominant clearly demonstrating the presence of turbulent flow structures along the jet attachment region. The distribution of the wall shear however varies as the jet angle ϕ increases from 30° to 90° .

Fig. 15 shows the effect of jet angle (ϕ) on average of Nu computed via (8) on the entire inclined surface for Reynolds number 5000, 10000 and 20000 with Case A boundary condition and $\beta = 0^\circ$. Based on curve fitting the following correlation of average Nu , Re and jet angle ϕ may be derived:

$$Nu_{avg} = A\phi^2 + B\phi + C \tag{11}$$

where $A = -(0.0436Re^2 + 0.021Re + 0.0081)$, $B = (5.56Re^2 + 2.77Re + 2.45)$, and $C = -(103.2Re^2 + 140.4Re - 130.8)$.

The effect of jet angle ϕ on heat transfer through the solid wall is more for high Re as compared to low Re . Numerical results for five different ϕ values (30° , 45° , 60° , 75° and 90°) show significant change in the heat transfer process as ϕ changes. Specifically, for a partic-

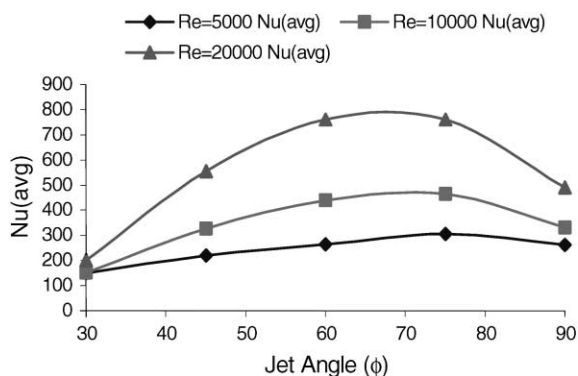


Fig. 15. Effect of jet angle ϕ on the non-dimensional heat transfer coefficient Nu_{avg} with $\beta = 0^\circ$.

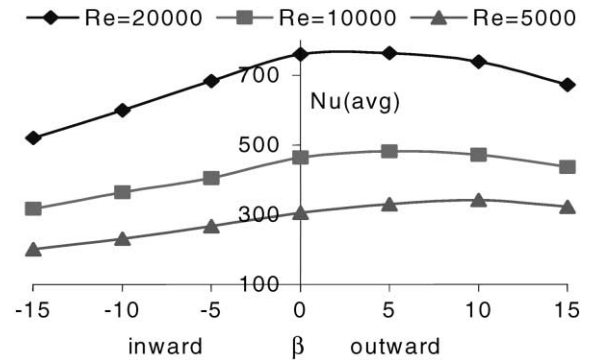


Fig. 16. Effect of jet angle β on the non-dimensional heat transfer coefficient Nu_{avg} with $\phi = 75^\circ$.

ular $Re = 20000$, the average Nusselt number varies from 187 at $\phi = 30^\circ$ to 775 at $\phi = 75^\circ$. For this geometric configuration, the plot predicts the highest Nu_{avg} of ~ 800 at $\phi = 70^\circ$. This contradicts the traditional understanding [21,22] that Nu_{avg} should occur when the jet is normal to the wall, i.e., at $\phi = 60^\circ$. This shift is due to bound vortices that bend the impinging jet and the close proximity of the wall boundaries and the small crotch angle α .

The angle β is inclination of jet axis in yz -plane as shown in Fig. 1. Jet angle β is varied from 5° to 15° (outward direction) and -5° to -15° (inward direction) in the yz -plane while ϕ is maintained at 75° . Fig. 16 documents the effect of β on Nu_{avg} . Increasing β in the inward direction reduces heat transfer for all Re . For lower Re , increasing β in the outward direction slightly improves the Nu_{avg} . However, for $Re = 20000$, Nu_{avg} sharply decreases as β is increased beyond 5° .

4. Conclusions

Jet impingement heat transfer and flow characteristics for two rectangular jets impinging upon an inclined surface have been studied with the following conclusions. Heat transfer is the maximum through the shear layer formed near the jet attachment stagnation region. The peak Nusselt number is always higher in Case A than in Case B for a particular inlet Reynolds number. This is primarily due to the fact that more energy is convected out through the openings in the latter case. Turbulence (velocity gradient) and wall shear force is higher in the shear layer region and the peak increases with the inlet Reynolds number. Documented correlations between Re and Nu_{avg} for both boundary conditions show that average Nu on the inside of the inclined surface increases as Re and/or Pr increases. Changing jet angle significantly affects the heat transfer process near the inclined surface. Specifically, increasing the jet im-

pingement angle ϕ can improve the Nu_{avg} by nearly four times for $Re = 20000$. For this geometric configuration resembling a vehicle windshield, an optimum ϕ exists for maximum heat transfer. However, increasing β reduces the heat transfer. The stagnation Nu has been correlated for the boundary condition of Case A that is substantially different than the previously reported Nu_{stg} for boundary condition similar to Case B. Finally, a correlation between Nu_{avg} , ϕ and Re has been presented.

Acknowledgements

This work was partially supported by NASA grant nos. NAG3-2520 and NAG3-2638 with D. Jacobson and D.R. Reddy as technical monitors, respectively.

References

- [1] P.J. Lamont, B.L. Hunt, The impingement of under expanded, axisymmetric jets on perpendicular and inclined plates, *J. Fluid Mech.* 100 (3) (1980) 471–511.
- [2] A. Benard, L.E. Brizzi, J.L. Bousgarbies, Study of several jets impinging on a plane wall: visualizations and laser velocimetry investigations, *J. Fluid Eng.* 121 (1999) 808–812.
- [3] S. Polat, B. Huang, A.S. Mujumdar, W.J.M. Douglas, Numerical flow and heat transfer under impinging jets: a review, *Ann. Rev. Numer. Fluid Mech. Heat Transfer* 2 (1989) 157–197.
- [4] H. Martin, Heat and mass transfer between impinging jets and solid surfaces, *Adv. Turbulence* 2 (1977) 37–44.
- [5] S.J. Downs, E.H. James, Jet impingement heat transfer—a literature survey, ASME paper no. 87-HT-35 (1987).
- [6] S.J. Lee, J.H. Lee, D.H. Lee, Local heat transfer measurements from an elliptical jet impinging on a flat plate using liquid crystal, *Int. J. Heat Mass Transfer* 37 (6) (1994) 967–976.
- [7] S.C. Arjocu, J.A. Liburdy, Identification of dominant heat transfer modes associated with the impingement of an elliptical jet array, *J. Heat Transfer* 122 (2000) 240–247.
- [8] H. Martin, Heat and mass transfer between impinging gas jets and solid surfaces, in: *Advances in Heat Transfer*, vol. 13, Academic Press, New York, 1977, pp. 1–60.
- [9] D.W. Colucci, R. Viskanta, Effect of nozzle geometry on local convective heat transfer to a confined impinging air jet, *Exp. Thermal Fluid Sci.* 13 (1996) 71–80.
- [10] Y. Pan, B.W. Webb, Visualization of local heat transfer under arrays of free-surface liquid jets, *Proc. Tenth Int. Heat Transfer Conf.* 4 (1994) 77–82.
- [11] D.E. Metzger, K.N. Cummings, W.A. Ruby, Effects of Prandtl number on heat transfer characteristics of impinging liquid jets, *Proc. Fifth Int. Heat Transfer Conf.* 2 (1974) 20–24.
- [12] M.M. Rahman, A.J. Bulla, J.E. Leland, Numerical model of conjugate heat transfer during free liquid jet impingement, *Proc. ASME, AES* 38 (1998) 475–486.
- [13] J.E. Leland, M.R. Pais, Free jet impingement heat transfer of a high Prandtl number fluid under conditions of highly varying properties, *J. Heat Transfer* 121 (1999) 592–597.
- [14] G.K. Morris, S.V. Garimella, R.S. Amano, Prediction of jet impingement heat transfer using a hybrid wall treatment with different turbulent Prandtl number functions, *J. Heat Transfer* 118 (1996) 562–568.
- [15] S. Roy, K. Nasr, P. Patel, B. Abdulnour, Rectangular jet impingement heat transfer on a vehicle windshield, *AIAA J. Thermophys. Heat Transfer* 16 (1) (2002) 154–157.
- [16] S. Roy, K. Nasr, P. Patel, B. Abdulnour, An experimental and numerical study of heat transfer off an inclined surface subject to an impinging airflow, *Int. J. Heat Mass Transfer* 45 (8) (2002) 1615–1629.
- [17] FLUENT® 5 User's guide, Fluent Inc., Lebanon, NH 1-4 (1998).
- [18] V. Yakhot, S.A. Orszag, Renormalization group analysis of turbulence. I. Basic theory, *J. Sci. Comput.* (1986) 3–51.
- [19] S.H. Lam, On the RNG theory of turbulence, *Phys. Fluids A* 4 (1992) 1007–1017.
- [20] Hyperworks® 4.0 Online users manual, Altair Engineering, Troy, MI (2000).
- [21] X. Yan, N. Saniei, Heat transfer from an obliquely impinging circular air jet to a flat plate, *Int. J. Heat Fluid Flow* 18 (1997) 591–599.
- [22] M.K. Lonney, J.J. Walse, Mean-flow and turbulent characteristics of free and impinging jet flows, *J. Fluid Mech.* 147 (1984) 397–429.